International Journal of Mass Spectrometry 309 (2012) 154–160

Contents lists available at SciVerse ScienceDirect

International Journal of Mass Spectrometry

journal homepage: www.elsevier.com/locate/ijms

Extracted fragment ion mobility distributions: A new method for complex mixture analysis

Sunyoung Lee, Zhiyu Li, Stephen J. Valentine, Steven M. Zucker, Nathaniel Webber, James P. Reilly, David E. Clemmer*

Department of Chemistry, Indiana University, Bloomington, IN 47405, United States

ARTICLE INFO

Article history:
Received 11 August 2011
Received in revised form
15 September 2011
Accepted 15 September 2011
Available online 22 September 2011

Keywords:
Ion mobility spectrometry
Collision-induced dissociation
Extracted ion chromatograms
Basic components from an extract of diesel
Phosphorylated peptide isomers

ABSTRACT

A new method is presented for constructing ion mobility distributions of precursor ions based upon the extraction of drift time distributions that are monitored for selected fragment ions. The approach is demonstrated with a recently designed instrument that combines ion mobility spectrometry (IMS) with ion trap mass spectrometry (MS) and ion fragmentation, as shown in a recent publication [J. Am. Soc. Mass Spectrom. 22 (2011) 1477–1485]. Here, we illustrate the method by examining selected charge states of electrosprayed ubiquitin ions, an extract from diesel fuel, and a mixture of phosphorylated peptide isomers. For ubiquitin ions, extraction of all drift times over small mass-to-charge (m/z) ranges corresponding to unique fragments of a given charge state allows the determination of precursor ion mobility distributions. A second example of the utility of the approach includes the distinguishing of precursor ion mobility distributions for isobaric, basic components from commercially available diesel fuel. Extraction of data for a single fragment ion is sufficient to distinguish the precursor ion mobility distribution of cycloalkyl-pyridine derivatives from pyrindan derivatives. Finally, the method is applied for the analysis of phosphopeptide isomers (LFpTGHPESLER and LFTGHPEpSLER) in a mixture. The approach alleviates several analytical challenges that include separation and characterization of species having similar (or identical) m/z values within complex mixtures.

1. Introduction

Because of its high-sensitivity, selectivity, and ability to generate information that can both identify and determine the structure of analytes, mass spectrometry (MS) has become an important technique for characterizing complex mixtures [1–4]. Two aspects of MS analyses limit the characterization of mixture components. One is the inability of MS to distinguish species of very similar (or identical) mass within the sample mixture [5]. Additionally, lower abundance ions may be masked by the presence of higher abundance species [6–8]. To some extent, increasing the experimental resolving power and instrumental mass accuracy can alleviate these problems. However, the need to characterize very complex samples such as those encountered in proteomics and metabolomics studies often requires a reduction of the sample complexity introduced into the mass spectrometer provided by liquid chromatography (LC) [4,9–13], gas chromatography (GC) [14,15], and, more recently, ion mobility spectrometry (IMS) [5,16–18] separation steps.

For experiments combining separation steps with MS, it is often desirable to obtain information regarding the retention and selectivity of specific sample components. For LC–MS and GC–MS experiments, this information is garnered by generating an extracted ion chromatogram (XIC) [19,20]. An XIC provides a chromatographic profile of a given species and is obtained from experiments in which all ions are examined by extracting the ion intensity associated with a specific mass-to-charge (m/z) species. This process can be simplified by fixing the mass spectrometer such that a specific m/z is monitored, thus, generating a selected ion chromatogram. In analogy with these chromatographic approaches, an extracted ion drift time distribution (XIDTD) can be obtained from nested IMS–MS data for a complex sample to generate the drift time distribution of a single ion [16]. The simplified selected ion monitoring approach can also be employed to record an IMS distribution for a single m/z species [21–23].

The specificity of XICs can be extended by utilizing tandem mass spectrometry (MS^n) data to monitor specific species. In this case, the mass spectrometer can be set to monitor fragment ions generating selected reaction monitoring (SRM) chromatograms [24]. In this paper we describe a new IMS–MS method that combines the concepts of XIDTD generation with SRM to improve the specificity of analyzing components from complex mixtures. The approach

* Corresponding author.
E-mail address: clemmer@indiana.edu (D.E. Clemmer).

1387-3806/$ – see front matter © 2011 Elsevier B.V. All rights reserved.
doi:10.1016/j.ijms.2011.09.011

utilizes a new drift tube/ion trap instrument that can select specific precursors and generate fragments by collision-induced dissociation (CID). A distribution that is produced from the highly specific precursor/fragment ion set is referred to as an extracted fragment ion drift time distribution (XFIDTD). We illustrate the method by examining several charge states of electrosprayed ubiquitin ions, where XFIDTDs generated from specific precursor and fragment ion sets are compared to XIDTDs generated from precursor ions and found to be nearly identical. Additionally, we use the new approach to delineate basic components of diesel and phophorylated peptide isomers. In these examples, the distributions cannot be obtained directly from precursor ion data (in the form of XIDTDs) because the components have identical mass. These techniques extend the foundation of parallel dissociation experiments by IMS that is becoming widely used [25–28]. Finally, we note that the approach is similar to experiments performed by Cooper and co-workers who demonstrated the extraction of compensation voltage (CV) distributions for select precursor and fragment ions by coupling field asymmetric waveform ion mobility spectrometry (FAIMS) with electron transfer dissociation (ETD) [29]. Two key differences are that the XFIDTD approach with IMS–MS techniques provides a better reproduction of the precursor ion distribution and this method provides structural information regarding the precursor ion while FAIMS dose not.

2. Experimental

2.1. General

IMS techniques [30–33], instrumentation [21–23,25–28,34–40], and theory [30,41–45] are described elsewhere. Additionally, the IMS/ion trap instrument used for the current studies is described in detail, elsewhere [46]. Thus, only a brief description of the apparatus is provided below. Fig. 1 shows a schematic diagram of the instrument used in these studies. Electrosprayed ions are desolvated in a differentially pumped region and then focused into an hour-glass ion funnel (F1) [39,47] where they are accumulated. Periodically an electrostatic gate is dropped and ions are released from the funnel into the drift tube, where they migrate ~1 m under the influence of a uniform drift field (~2.3×10^3 V m^{-1}) through ~3 Torr of an inert buffer gas mixture (see below). As the packet of ions migrates through the drift region, different species separate according to differences in their mobilities through the buffer gas. As ions approach the exit of the drift tube they must pass through a second gate (that is opened at a specific delay time relative to the release pulse); those ions that have the appropriate mobilities are then transferred through a second ion funnel (F2), that focuses the diffuse ion cloud in order to allow it to pass through the exit aperture and into the LTQ Velos instrument (Thermo Electron, San Jose, CA).

Upon entering the LTQ, an rf guide is used to direct ions into the linear ion trap mass analyzer. Once inside the trap, the mobility-selected species are stored, mass analyzed, and periodically subjected to MS/MS analyses using CID (see below).

2.2. Obtaining IMS distributions

IMS distributions are generated by scanning a drift time (t_D) selection time. This is accomplished by establishing a delay time between the introduction and selection gates (Fig. 1). By recording the ion signal as this delay time is scanned across the total t_D range it is possible to obtain the IMS distribution. In the current instrumentation configuration, the introduction gate is pulsed at a frequency of 55 Hz and the delay time is scanned from ~10 to ~25 ms using time increments of ~80 to ~150 μs. The relatively long t_D values result from the use of a buffer gas mixture.

For both XIDTD and XFIDTD experiments, a total of 500 ms of ion injection time has been used and 20 scans are averaged to obtain a single mobility selection data point. Therefore, ~20 min are required to obtain one dataset across a 12-ms drift time range employing 100 μs steps.

2.3. Buffer gas composition

The buffer gas in the IMS region is primarily a mixture of helium and nitrogen. For these experiments helium is introduced into the drift tube near F2. In the desolvation region, a small portion of gas from atmosphere is leaked into the drift tube. This provides two benefits for the experiments. First, an increased ion signal level is obtained as the ion source gas influx aids transport of ions into the trapping region of the hour-glass ion funnel (F1). Additionally, the buffer gas mixture supports a higher drift voltage providing increased resolving power for this drift tube.

A disadvantage of the gas mixture is that collision cross sections cannot be obtained for given ions. Additionally, mobility distributions can be broadened due to interaction with small amounts of other molecules such as H_2O from atmosphere [48,49]. That said, the improvement in resolving power due to the increased field is greater than such losses as indicated by the fact that the resolution obtained here approaches that obtained for a drift tube that is twice as long employing pure He. Finally, the mobility distributions obtained on the current instrument are nearly identical to those obtained on instruments utilizing He buffer gas. Thus, the relative mobilities (relative collision cross sections) for different ions can be determined.

2.4. Ion dissociation

As mentioned above, ions are mobility selected by setting the delay time of the selection gate relative to the introduction gate. Ions selected in this manner are stored in the linear trap and they can be dissociated by collisional activation. The stored ions are collisionally activated by applying a resonant rf excitation waveform for 10 ms with activation q of 0.25 and normalized collision energy of 25%, 38%, and 22% for ubiquitin ions, basic compound ions from the diesel sample, and phosphopeptides, respectively. Then, the MS^2 mass spectrum is subsequently scanned. In order to get better signal intensities of MS^2 fragments, the ion injection time has been set to 8 s with the automatic gain control off. Mass selection is employed (±1 Th) prior to the ion dissociation step.

2.5. Sample preparation and ionization

Bovine ubiquitin (90% purity) has been obtained from Sigma–Aldrich (St. Louis, MO) and used without further purification. The diesel sample (#2 diesel) has been provided as a gift from C&S Petroleum Products (Bloomington, IN). The electrospray solution of 2.3×10^{-5} M ubiquitin is prepared in 49:49:2 (vol.%) water:methanol:acetic acid. The solution of diesel is prepared as follows. 1 mL of diesel is mixed with a 2-mL aliquot of 50% aqueous methanol with 3% acetic acid for 30 s by vortexing (Vortex Genie 2, FisherScientific, Bohemia, NY). The methanol/water extract was vacuum dried using a centrifugal concentrator (CentriVap, Labconco Co., Kansas City, MI) and dissolved with 0.2 mL of methanol with 1% acetic acid. The synthetic phosphopeptides LFpTGHPESLER and LFTGHPEpSLER have been generously provided by Professor G.E. Reid (Michigan State University, East Lansing, MI) and the 1:1 mixture of two phosphopeptides is prepared in 50:49:1 (vol.%) methanol:water:acetic acid solution to provide a final concentration of 25 μM for each isomer. The solutions are infused through

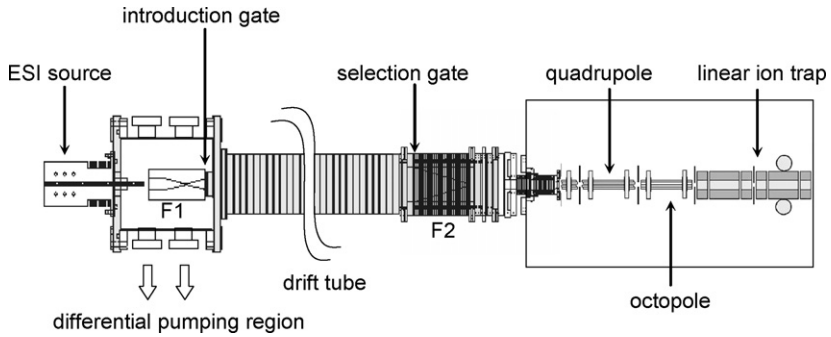

Fig. 1. Schematic diagram of the IMS–MS instrument. The instrument is comprised of an ESI source/drift tube assembly that is coupled to the front of a LTQ Velos instrument (Thermo Electron, San Jose, CA). The drift tube contains a combination of ion gates (introduction and selection) and ion funnels (F1 and F2).

a pulled capillary (75 μm i.d., 360 μm o.d.) tip at a flow rate of 0.30 μL min^{-1} using a syringe pump (KD Scientific, Holliston, MA). The capillary tip is maintained at a DC bias of ~2.0 kV above the voltage of the entrance plate to the desolvation region.

3. Results and discussion

3.1. Example IMS–MS datasets

The coupling of the drift tube to a linear trap requires that ion mobility distributions are collected in a scanning mode where ion intensities are recorded at defined selection times (see above). This approach is less efficient than our combination of IMS with time-of-flight (TOF) MS [37]. In that IMS/MS approach, the flight times of all ions are nested within the t_D measurements and recorded in a single experimental sequence. Despite the difference in the measurement approach used here, the quality of the data is very similar.

Fig. 2 shows the IMS–MS distribution obtained using the new instrument for electrosprayed $[M+nH]^{n+}$ ions of ubiquitin (in this case n = 6–13). The gas-phase conformations of different charge states are observed at different ranges in t_D. For example, for $[M+13H]^{13+}$ ions, a single feature that is ~500 μs wide (t_D) is observed. In comparison, multiple features spanning a range of ~4 ms (t_D) are observed for $[M+8H]^{8+}$ ions. This is consistent with previous studies showing a transition from compact and partially folded conformations associated with lower charge states to more elongated structures associated with higher charge states [50–52]. Drift time distributions for all charge states show a significant degree of overlap as can be observed from the broad, unresolved drift time distribution ranging from ~14 to ~20 ms shown in Fig. 2.

3.2. Comparison of precursor ion XIDTDs and fragment ion XFIDTDs

As mentioned above, XIDTDs of precursor ions can be generated by integrating all m/z charge points across a narrow range at each t_D delay setting. Fig. 3 shows distributions for the $[M+7H]^{7+}$, $[M+10H]^{10+}$, and $[M+12H]^{12+}$ precursor ubiquitin ions. To obtain XFIDTDs that resemble the XIDTDs it is necessary that different gas-phase conformations of these precursor ions exhibit the same proclivity for formation of the selected fragment ion. That is, formation of the product ion cannot be more energetically favorable for specific conformations. Additionally, for a sample containing many different ions such as the multiple charge states of the ubiquitin system, the degree of relatedness also depends on the ability to generate unique fragments for specific precursor charge states.

For the different charge states of ubiquitin ions, distinctive fragment ions can be selected. Fig. 3 shows MS^2 spectra for the $[M+7H]^{7+}$, $[M+10H]^{10+}$, and $[M+12H]^{12+}$ ubiquitin ions. The fragment ion (CID) spectrum generated from $[M+7H]^{7+}$ ions shows that the main features range from ~900 to ~1400 m/z. Dominant spectral features are observed at higher m/z values including the $y_{58}{}^{5+}$ to $y_{62}{}^{5+}$ homologous series of ions. The fragment ion spectrum generated from $[M+10H]^{10+}$ ions shows features ranging from ~600 to ~1100 m/z. Dominant spectral features are observed in the ~800 to ~1000 m/z range. Several of the higher abundance peaks include the $y_{58}{}^{8+}$, $y_{58}{}^{7+}$, $y_{59}{}^{7+}$, and $b_{52}{}^{6+}$ ions. The fragment ion spectrum generated from the $[M+12H]^{12+}$ ions shows features ranging from ~500 to ~1000 m/z with the most dominant features occurring between ~600 and ~850 m/z. The y_{58} fragment is again observed as some of the more intense features existing as the 8+, 9+, and 10+ charge states.

Because of its relatively high prevalence in the three different MS^2 spectra, the y_{58} fragment has been selected to create the XFIDTD. The selection is also favored because this fragment exists as a unique charge state within each MS^2 spectrum. Consider the fragmentation spectrum generated from the $[M+7H]^{7+}$ ubiquitin ions.

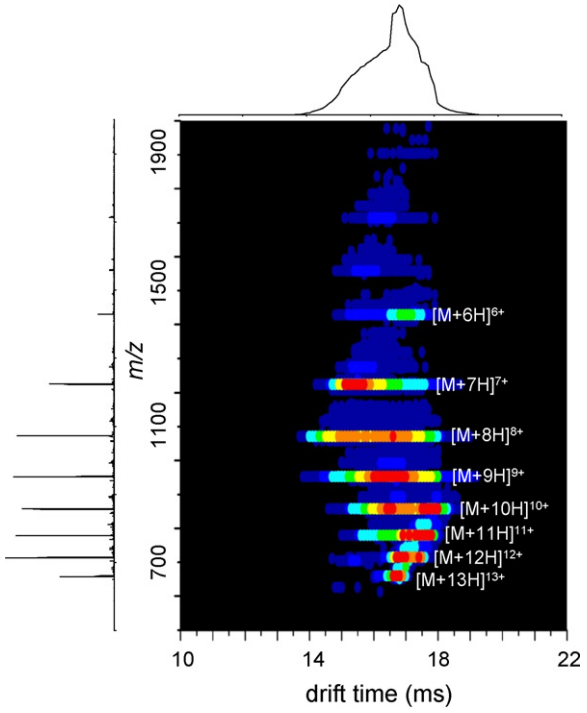

Fig. 2. t_D (m/z) dotplot showing the multiply charged $[M+nH]^{n+}$ ubiquitin ions (n = 6–13). The total t_D distribution shown across the top is obtained by integrating data points across the entire m/z range for each t_D bin. The mass spectrum shown on the left is obtained by integrating data points across all t_D values for each m/z value.

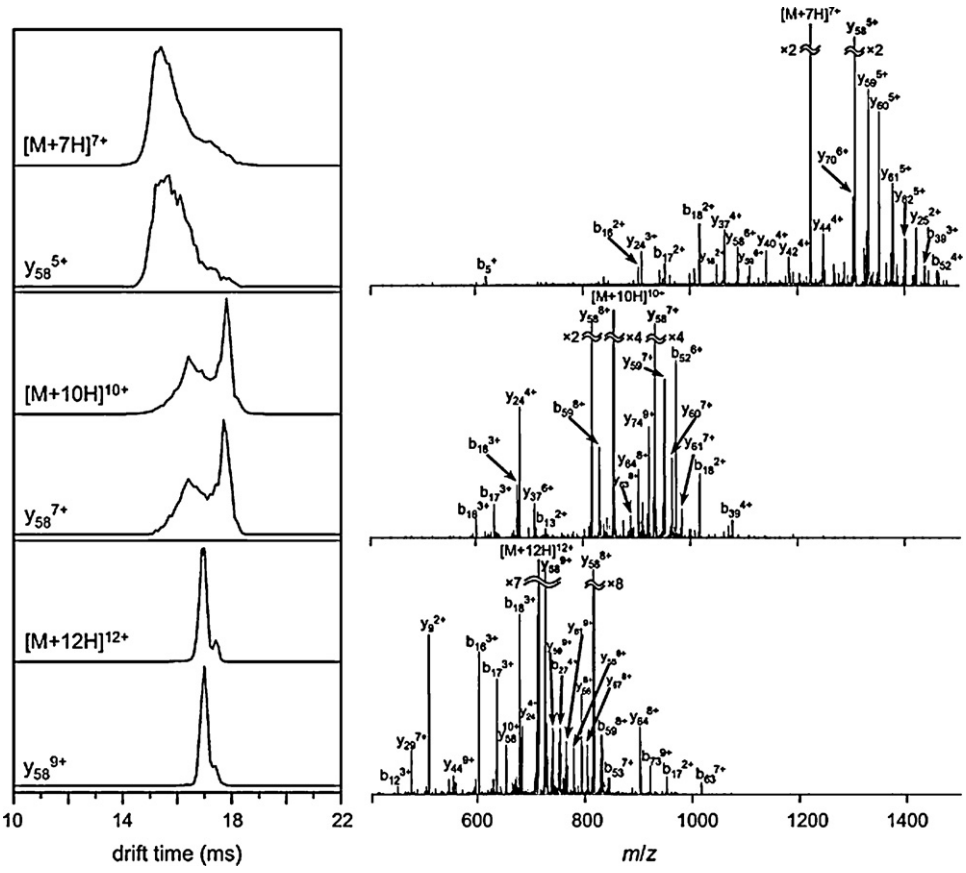

Fig. 3. t_D distributions (left panel) obtained for the precursor (XIDTD) and fragment (XFIDTD) ions of the $[M+7H]^{7+}$, $[M+10H]^{10+}$, and $[M+12H]^{12+}$ charge states of ubiquitin. Distributions are obtained by integrating all m/z points across a narrow range for each t_D bin from a t_D (m/z) dataset (e.g., Fig. 1). XIDTD and XFIDTD distributions are obtained from MS and MS^2, respectively. The top two traces show a comparison of the XIDTD obtained for the $[M+7H]^+$ ubiquitin ions and the XIFDTD obtained from the $y_{58}{}^{5+}$ ions generated by fragmentation of the $[M+7H]^+$ ions. The middle and bottom two traces show the same comparison for the $[M+10H]^{10+}$ and $[M+12H]^{12+}$ charge states and their respective fragment ions ($y_{58}{}^{7+}$ and $y_{58}{}^{9+}$) used to create the XFIDTDs. The CID mass spectra shown on the right are obtained at ~15.4, ~17.8, and ~17.0 ms for the $[M+7H]^{7+}$, $[M+10H]^{10+}$, and $[M+12H]^{12+}$ ions, respectively. Major fragments are assigned in the CID mass spectra.

Here, the $y_{58}{}^{5+}$ ion is utilized to generate the XFIDTD because it is observed for this charge state and not the others. Fig. 3 shows the t_D distributions generated by extraction of the data for the $[M+7H]^{7+}$ precursor ions and the $y_{58}{}^{5+}$ fragment ions. The XIDTD and XFIDTD are nearly identical exhibiting a relatively broad feature with a peak maximum at 15.40 ms. A shoulder at 17.20 ms observed in both t_D distributions indicates the presence of gas-phase conformations of lower mobilities. A difference in the two distributions is the increased noise associated with the XFIDTD compared with the XIDTD. This presumably is a result of the decreased ion signal associated with the fragment ion compared to that of the precursor ion.

The XIDTDs and XFIDTDs generated from the other charge states are also observed to be very similar and are shown in Fig. 3. For example, for the $[M+10H]^{10+}$ precursor ions, the XIDTD shows the presence of two, partially resolved features. A broad feature indicating the presence of multiple conformations is observed with a peak maximum at 16.40 ms. A narrow feature corresponding to more elongated ions is also observed at 17.80 ms. The XFIDTD obtained for the $y_{58}{}^{7+}$ ions obtained upon activation of $[M+10H]^{10+}$ precursor ions, shows a nearly identical distribution. The XIDTD for the $[M+12H]^{12+}$ precursor ions is comprised of two relatively narrow features centered at 17.00 and ~17.40 ms. The higher mobility peak exhibits greater intensity. The XFIDTD obtained for the $y_{58}{}^{9+}$ ions obtained upon activation of $[M+12H]^{12+}$ precursor ions, shows a nearly identical distribution with the same relative intensities.

This simple, proof-of-concept study demonstrates that the two criteria for using XFIDTDs are easily satisfied. That is, unique fragment m/z values are readily generated from precursor ions and the fragmentation is not dependent on the conformation from which they are generated [53]. While we have chosen this system such that there are unique m/z values associated with the fragment ions, this need not be the case. We could just as easily have created these unique IMS distributions from an identical m/z fragment ion (assuming it is formed) as long as we started with a unique precursor ion. Thus, it is possible to produce a unique IMS distribution from any of the precursor/fragment ion pairs that are associated with the ion.

3.3. XFIDTDs obtained for basic components of diesel fuel

It is instructive to consider the determination of IMS distributions for specific ions from a mixture by using the XFIDTD approach. Here, individual IMS profiles for isomeric, basic components from diesel fuel are determined. Upon electrospraying the aqueous extract from diesel we find a number of basic components ranging from $m/z = 100$ to 300. Basic, nitrogen-containing compounds such as pyridine derivatives have been determined to comprise a portion of diesel fuel; additionally, multiple pyridine derivatives can exist as isomers with m/z value of 230 [54]. In this demonstration, the mass spectral peak at $m/z = 230$ (one of the higher abundant features) has been examined.

Fig. 4a shows the XIDTD for the $[M+H]^+$ precursor ions comprising the feature at $m/z = 230$. The broad distribution obtained from the XIDTD suggests that multiple isomers of pyridine derivative compounds may exist at this m/z value. Two main features

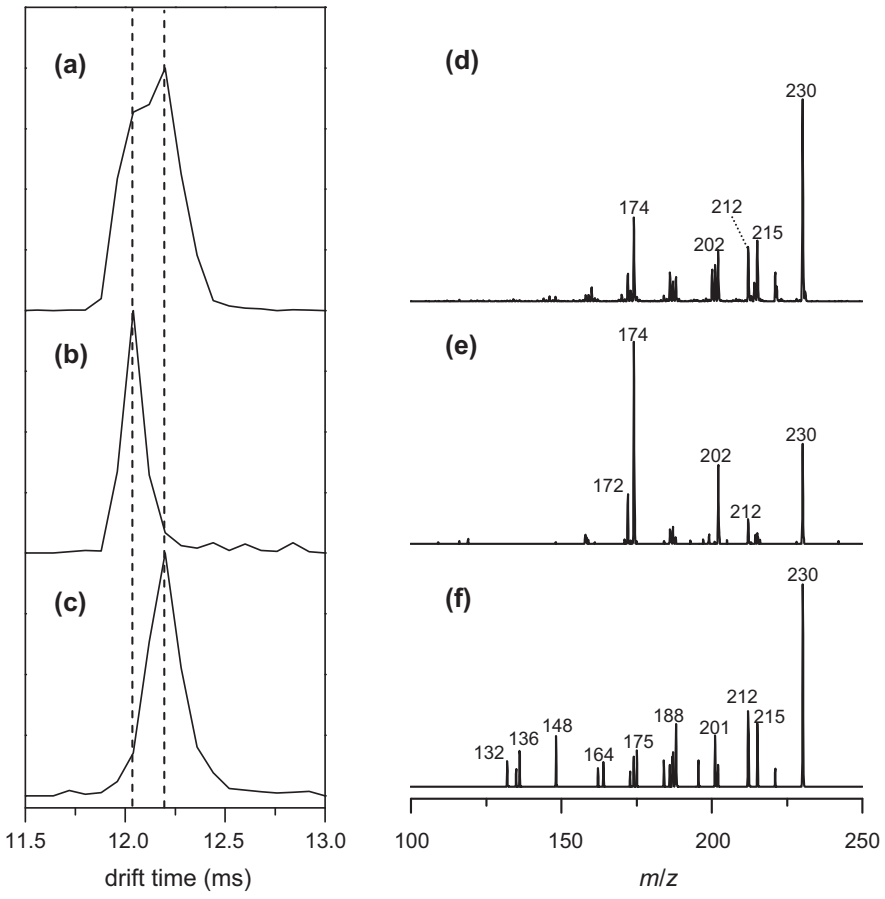

Fig. 4. (a) t_D distribution (XIDTD) of the $[M+H]^+$ ions (m/z = 230) of basic components from the aqueous extract of diesel fuel. XFIDTDs obtained for the CID fragments at (b) m/z = 202 and (c) 215. The CID mass spectra shown on the right are obtained (d) without mobility separation and at drift selection times of (e) 11.96 and (f) 12.52 ms.

centered at 12.04 and 12.20 ms are observed, indicating partially resolved species containing similar mobilities. Complete resolution of these ions is intractable with the resolving power of our IMS instrument. Beyond that, even though some components may be partially resolved in the mobility separation, assigning mobilities is still somewhat ambiguous because the ESI mass spectrum is the same for each feature in the t_D distribution of the mixture.

To further characterize this system the precursor ions have been collisionally activated to produce characteristic fragment ions. The CID spectrum of specific mobility ions shows a unique fragmentation pattern that can be used as a molecular fingerprint to distinguish components within the mixture as well as to help identify molecular classes. From the aqueous extract of diesel, the precursor ions at m/z = 230 have been isolated in the ion trap and fragmented by CID. The CID spectrum of all precursor ions at m/z = 230 is shown in Fig. 4d. The MS^2 spectrum obtained at a t_D selection of 11.96 ms shows a couple of dominant peaks at m/z = 174 and 202 (Fig. 4e). There is no fragment ion below m/z = 170. In contrast to the high-mobility ions, the CID spectrum of the low-mobility ions at a t_D selection of 12.52 ms shows a more complicated fragmentation pattern including fragments with small m/z values (m/z < 170). The distinctive fragments for the low-mobility ions appear at m/z = 132, 136, 148, 164, 175, 188, 201, and 215 (Fig. 4f). Because the CID fragments at m/z = 202 and 215 are unique to the high- and low-mobility ions, respectively, they are used to generate the XFIDTDs. As shown from the XFIDTDs in Fig. 4c and d, the centers of the features in these t_D distributions are slightly offset. The different XFIDTDs suggest that there are at least two different types of molecules for the precursor ions with a value of m/z = 230.

As mentioned above, the CID of the low-mobility ions produce more fragments than activation of the high-mobility ions. Based on the distinct fragmentation patterns obtained at different t_D selections it is possible to propose two groups of molecules for assignment to specific mobility ions. Among the isomers of pyridine derivative compounds, it is possible that the high-mobility ions with m/z = 230 correspond to pyrindan derivatives that consist of fused rings. Additionally, it can be considered that the low-mobility ions are related to cycloalkyl pyridine derivatives. Under the same dissociation conditions, more fragments would be expected from cycloalkyl pyridine derivatives compared to pyrindan derivatives because the fused-ring compounds would require cleavage of two bonds to produce fragments. Also, it might be expected that the cross section of the constrained fused-ring structure would be more compact than that of a more linear structure of linked rings. This explanation would suggest that the pyrindan derivative ions have a slightly higher mobility than the cycloalkyl pyridine ions, as shown in Fig. 4. In summary, it is not possible to assign the relative mobilities of ions of specific molecular classes from an analysis of the diesel component mixture. However, the XFIDTDs obtained from distinct dissociation fragments can be useful to determine the presence of particular components within the mixture.

3.4. XFIDTDs obtained for phosphopeptide isomers

Another attractive system that can be analyzed with the XFIDTD method is a mixture of peptide isomers formed by post-translation modification such as phosphorylation. Two model synthetic phosphorylated peptide isomers (LFpTGHPESLER and LFTGHPEpSLER) having the same sequence but different phosphorylation sites have

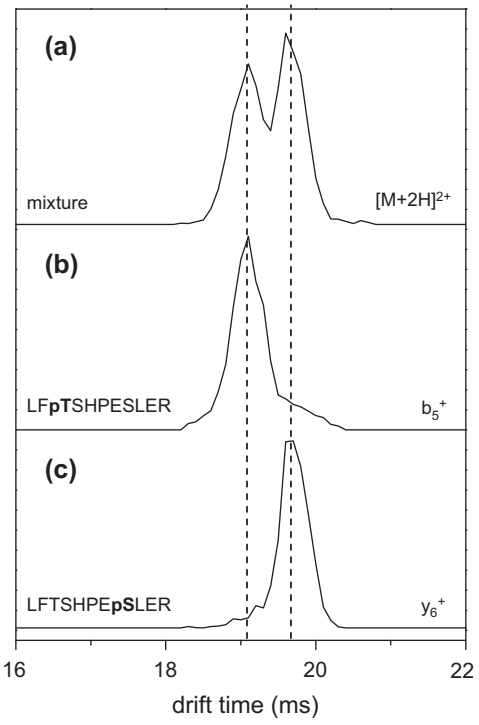

Fig. 5. (a) t_D distribution (XIDTD) of the $[M+2H]^{2+}$ ions (m/z = 683) of phosphopeptide isomers, LFpTGHPESLER and LFTGHPEpSLER. XFIDTDs obtained for the CID fragments at (b) m/z = 636 and (c) 810 that correspond to b_5^+ and y_6^+ ions, respectively.

been examined using the XFIDTD approach. Fig. 5a shows the XIDTD for the $[M+2H]^{2+}$ precursor ions (m/z = 683) obtained upon electrospraying the isomer mixture. Two features at 19.1 and 19.6 ms are partially resolved. However, it is not possible to assign the phosphopeptides with IMS–MS alone due to the identical m/z value of the precursor ions.

Each of the phosphopeptides has been previously studied using CID in a linear ion trap [55]. The CID spectra for each phosphopeptide present distinct fragmentation patterns. Two notable fragments that can be used to distinguish the phosphopeptide isomers are the b_5^+ and y_6^+ ions (m/z = 636 and 810, respectively) for the LFpTGHPESLER and LFTGHPEpSLER species, respectively. From the XFIDTD analysis, the intensities of these fragments vary across the t_D range. From the MS^2 data, the distinctive fragment containing the phosphorylated threonine residue (b_5^+) first appears at an earlier t_D selection (18.3 ms), while the fragment containing the phosphoyrlated serine residue (y_6^+) is first noticeable at 19.2 ms. The b_5^+ and y_6^+ ions reach their maximum intensities at t_D selections of 19.1 and 19.6 ms, respectively. The XFIDTD profiles for the indicative fragments are shown in Fig. 5b and c. This analysis suggests that the mobility of $[M+2H]^{2+}$ LFpTGHPESLER ions is higher than that of $[M+2H]^{2+}$ LFTGHPEpSLER ions. Additionally, the unique CID fragments for each phosphopeptide allow the identification of the individual isomers from a mixture.

3.5. Comparison of XFIDTD analysis to FAIMS–ETD studies

Above we have demonstrated the utility of characterizing components in mixtures with XFIDTD analysis. We note that although this work is here presented as a new method for IMS–MS experiments, a similar approach has been described for FAIMS. Cooper and co-workers have recently applied high-field asymmetric waveform ion mobility spectrometry (FAIMS) coupled with electron transfer dissociation (ETD) mass spectrometry for the analysis of phosphopeptides [29]. The FAIMS separation prior to ion fragmentation helps to distinguish the phosphopeptide isomers. However, the extracted CV distributions from the FAIMS–ETD analysis show a lack of reproducibility and consequently it is difficult to determine the precursor ion distributions. In the FAIMS study, the extracted CV data for the $[M+3H]^{3+}$ precursor ions of the peptide APLpSFRGSLPKSYVK present a different profile compared to the extracted CV distributions for ETD fragments obtained from the same peptide ion. Additionally, because of the field conditions employed by FAIMS separations it is not possible to obtain structural information in the form of collision cross sections.

From the analysis above, the advantages of the XFIDTD method compared with FAIMS are apparent. It is noteworthy that the performance of CID after the mobility separation not only allows for distinguishing precursor ions but also provides a means of ion identification. Further study on the analysis of complex mixtures with the XFIDTD approach may include coupling IMS selection with various dissociation methods. Previous work has shown that ultraviolet photodissociation yields multiple unique fragments including many cross-ring cleavages for glycan and carbohydrate isomer ions [46,56]. New IMS–MS instrumentation that employ a range of dissociation methods would extend the XFIDTD approach allowing detailed analyses into individual components of complex mixtures. It is noted that a limitation of such analyses is that the XFIDTD requires the existence of at least one unique precursor/fragment ion pair.

4. Conclusions

A new method for analyzing complex mixtures that cannot be resolved by MS and IMS–MS analysis alone has been demonstrated. The new approach relies on the production of unique fragment ions for mobility-selected precursor ions. By integrating all ions at each t_D bin over a limited m/z range, fragment ion t_D distributions can be created that are representative of the mobility distributions of precursor ions. The new technique may find unique applications in the study of complicated mixtures containing isomers and different gas-phase ion conformers.

Acknowledgements

The authors thank Professor Gavin E. Reid (Michgan State University) for providing the phosphorylated peptides. We also acknowledge support for the development of new instrumentation by a grant from the National Institutes of Health (1RC1GM090797-02).

References

[1] M.T. Bowers, A.G. Marshall, F.W. McLafferty, Mass spectrometry: recent advances and future directions, J. Phys. Chem. 100 (1996) 12897–12910.
[2] A.G. Marshall, R.P. Rodgers, Petroleomics: the next grand challenge for chemical analysis, Acc. Chem. Res. 37 (2004) 53–59.
[3] Y. Park, C.B. Lebrilla, Application of Fourier transform ion cyclotron resonance mass spectrometry to oligosaccharides, Mass Spectrom. Rev. 24 (2005) 232–264.
[4] W.J. Griffiths, Y. Wang, Mass spectrometry: from proteomics to metabolomics and lipidomics, Chem. Soc. Rev. 38 (2009) 1882–1896.
[5] M.D. Plasencia, D. Isailovic, S.I. Merenbloom, Y. Mechref, D.E. Clemmer, Resolving and assigning N-linked glycan structural isomers from ovalbumin by IMS–MS, J. Am. Soc. Mass Spectrom. 19 (2008) 1706–1715.
[6] R.D. Smith, G.A. Anderson, M.S. Lipton, L. Pasa-Tolic, Y. Shen, H.R. Udseth, The use of accurate mass tags for high-throughput microbial proteomics, OMICS 6 (2002) 61–90.
[7] A.E. Counterman, A.E. Hilderbrand, C.A. Srebalus Barnes, D.E. Clemmer, Formation of peptide aggregates during ESI: size, charge, composition, and contributions to noise, J. Am. Soc. Mass Spectrom. 12 (2001) 1020–1035.
[8] X. Liu, S.J. Valentine, M.D. Plasencia, S. Trimpin, S. Naylor, D.E. Clemmer, Mapping the human plasma proteome by SCX–LC–IMS–MS, J. Am. Soc. Mass Spectrom. 18 (2007) 1249–1264.

[9] D.A. Wolters, M.P. Washburn, J.R. Yates, An automated multidimensional protein identification technology for shotgun proteomics, Anal. Chem. 73 (2001) 5683–5690.
[10] J. Peng, J.E. Elias, C.C. Thoreen, L.J. Licklider, S.P. Gygi, Evaluation of multidimensional chromatography coupled with tandem mass spectrometry (LC/LC–MS/MS) for large-scale protein analysis: the yeast proteome, J. Proteome Res. 2 (2003) 43–50.
[11] Y. Shen, J.M. Jacobs, D.G. Camp, I.I. Rang, R.J. Moore, R.D. Smith, W. Xiao, R.W. Davis, R.G. Tompkins, Ultra-high-efficiency strong cation exchange LC/RPLC/MS/MS for high dynamic range characterization of the human plasma proteome, Anal. Chem. 76 (2004) 1134–1144.
[12] J.E.P. Syka, J.A. Marto, D.L. Bai, S. Horning, M.W. Senko, J.C. Schwartz, B. Ueberheide, B. Garcia, S. Busby, T. Muratore, J. Shabanowitz, D.F. Hunt, Novel linear quadrupole ion trap/FT mass spectrometer: performance characterization and use in the comparative analysis of histone H3 post-translational modifications, J. Proteome Res. 3 (2004) 621–626.
[13] X. Wang, M.R. Emmett, A.G. Marshall, Liquid chromatography electrospray ionization Fourier transform ion cyclotron resonance mass spectrometric characterization of N-linked glycans and glycopeptides, Anal. Chem. 82 (2010) 6542–6548.
[14] O. Fiehn, J. Kopka, R.N. Trethewey, Identification of uncommon plant metabolites based on calculation of elemental compositions using gas chromatography and quadrupole mass spectrometry, Anal. Chem. 72 (2000) 3573–3580.
[15] E.M. Lenz, I.D. Wilson, Analytical strategies in metabonomics, J. Proteome Res. 6 (2007) 443–458.
[16] J.A. Taraszka, A.E. Counterman, D.E. Clemmer, Gas-phase separations of complex tryptic peptide mixtures, Fresenius J. Anal. Chem. 369 (2001) 234–245.
[17] K. Tang, F. Li, A.A. Shvartsburg, E.F. Strittmatter, R.D. Smith, Two-dimensional gas-phase separations coupled to mass spectrometry for analysis of complex mixtures, Anal. Chem. 77 (2005) 6381–6388.
[18] E. Duijin, A. Barendregt, S. Synowsky, C. Versluis, A.J. Heck, Chaperonin complexes monitored by ion mobility mass spectrometry, J. Am. Chem. Soc. 131 (2009) 1452–1459.
[19] C.R. Borges, Concept for facilitating analyst-mediated interpretation of qualitative chromatographic-mass spectral data: an alternative to manual examination of extracted ion chromatograms, Anal. Chem. 79 (2007) 4805–4813.
[20] L.A. Hammad, M.M. Saleh, M.V. Novotny, Y. Mechref, Multiple-reaction monitoring liquid chromatography mass spectrometry for monosaccharide compositional analysis of glycoproteins, J. Am. Soc. Mass Spectrom. 20 (2009) 1224–1234.
[21] D. Wittmer, B.K. Luckenbill, H.H. Hill, Y.H. Chen, Electrospray-ionization ion mobility spectrometry, Anal. Chem. 66 (1994) 2348–2355.
[22] D.E. Clemmer, R.R. Hudgins, M.F. Jarrold, Naked protein conformations: cytochrome *c* in the gas phase, J. Am. Chem. Soc. 117 (1995) 10141–10142.
[23] G. von Helden, T. Wyttenbach, M.T. Bowers, Conformation of macromolecules in the gas phase: use of matrix-assisted laser desorption methods in ion chromatography, Science 267 (1995) 1483–1485.
[24] S. Gallien, E. Duriez, B. Domon, Selected reaction monitoring applied to proteomics, J. Mass. Spectrom. 46 (2011) 298–312.
[25] C.S. Hoaglund-Hyzer, J. Li, D.E. Clemmer, Mobility labeling for parallel CID of ion mixtures, Anal. Chem. 72 (2000) 2737–2740.
[26] S.J. Valentine, S.L. Koeniger, D.E. Clemmer, A split-field drift tube for separation and efficient fragmentation of biomolecular ions, Anal. Chem. 75 (2003) 6202–6208.
[27] E.S. Baker, K.Q. Tang, W.F. Danielson III, D.C. Prior, R.D. Smith, Simultaneous fragmentation of multiple ions using IMS drift time dependent collision energies, J. Am. Soc. Mass Spectrom. 19 (2008) 411–419.
[28] W.J. Sun, J.C. May, D.H. Russell, A novel surface-induced dissociation instrument for ion mobility-time-of-flight mass spectrometry, Int. J. Mass Spectrom. 259 (2007) 79–86.
[29] Y. Xuan, A.J. Creese, J.A. Horner, H.J. Cooper, High-field asymmetric waveform ion mobility spectrometry (FAIMS) coupled with high-resolution electron transfer dissociation mass spectrometry for the analysis of isobaric phosphopeptides, Rapid Commun. Mass Spectrom. 23 (2009) 1963–1969.
[30] E.A. Mason, E.W. McDaniel, Transport Properties of Ions in Gases, Wiley, New York, 1988.
[31] D.E. Clemmer, M.F. Jarrold, Ion mobility measurements and their applications to clusters and biomolecules, J. Mass Spectrom. 32 (1997) 577–592.
[32] R.H.St. Louis, H.H. Hill, Ion mobility spectrometry in analytical chemistry, Crit. Rev. Anal. Chem. 21 (1990) 321–355.
[33] C.S. Hoaglund-Hyzer, A.E. Counterman, D.E. Clemmer, Anhydrous protein ions, Chem. Rev. 99 (1999) 3037–3079.
[34] S. Myung, E.R. Badman, Y.J. Lee, D.E. Clemmer, Structural transitions of electrosprayed ubiquitin ions stored in an ion trap over ~10 ms to 30 s, J. Phys. Chem. A 106 (2002) 9976–9982.
[35] Y.H. Chen, W.F. Siems, H.H. Hill Jr., Fourier transform electrospray ion mobility spectrometry, Anal. Chim. Acta 334 (1996) 75–84.
[36] K.J. Gillig, B. Ruotolo, E.G. Stone, D.H. Russell, K. Fuhrer, M. Gonin, A.J. Schultz, Coupling high-pressure MALDI with ion mobility/orthogonal time-of-flight mass spectrometry, Anal. Chem. 72 (2000) 3965–3971.
[37] C.S. Hoaglund, S.J. Valentine, C.R. Sporleder, J.P. Reilly, D.E. Clemmer, Three-dimensional ion mobility/TOFMS analysis of electrosprayed biomolecules, Anal. Chem. 70 (1998) 2236–2242.
[38] C.S. Hoaglund-Hyzer, D.E. Clemmer, Ion trap/ion mobility/quadrupole/time-of-flight mass spectrometry for peptide mixture analysis, Anal. Chem. 73 (2001) 177–184.
[39] K. Tang, A.A. Shvartsburg, H.N. Lee, D.C. Prior, M.A. Buschbach, F.M. Li, A.V. Tolmachev, G.A. Anderson, R.D. Smith, High-sensitivity ion mobility spectrometry/mass spectrometry using electrodynamic ion funnel interfaces, Anal. Chem. 77 (2005) 3330–3339.
[40] M.E. Belov, B.H. Clowers, D.C. Prior, W.F. Danielson III, A.V. Liyu, B.O. Petritis, R.D. Smith, Dynamically multiplexed ion mobility time-of-flight mass spectrometry, Anal. Chem. 80 (2008) 5873–5883.
[41] H.E. Revercomb, E.A. Mason, Theory of plasma chromatography/gaseous electrophoresis – a review, Anal. Chem. 47 (1975) 970–983.
[42] E. Mack, Average cross-sectional areas of molecules by gaseous diffusion methods, J. Am. Chem. Soc. 47 (1925) 2468–2482.
[43] A.A. Shvartsburg, M.F. Jarrold, An exact hard-spheres scattering model for the mobilities of polyatomic ions, Chem. Phys. Lett. 261 (1996) 86–91.
[44] M.F. Mesleh, J.M. Hunter, A.A. Shvartsburg, G.C. Schatz, M.F. Jarrold, Structural information from ion mobility measurements: effects of the long-range potential, J. Phys. Chem. 100 (1996) 16082–16086.
[45] T. Wyttenbach, G. von Helden, J.J. Batka, D. Carlat, M.T. Bowers, Effect of the long-range potential on ion mobility measurements, J. Am. Soc. Mass Spectrom. 8 (1997) 275–282.
[46] S.M. Zucker, S. Lee, N. Webber, S.J. Valentine, J.P. Reilly, D.E. Clemmer, An ion mobility/ion trap/photodissociation instrument for characterization of ion structure, J. Am. Soc. Mass Spectrom. 83 (2011) 1477–1485.
[47] S.A. Shaffer, D.C. Prior, G.A. Anderson, H.R. Udseth, R.D. Smith, An ion funnel interface for improved ion focusing and sensitivity using electrospray ionization mass spectrometry, Anal. Chem. 70 (1998) 4111–4119.
[48] G.R. Asbury, H.H. Hill Jr., Using different drift gases to change separation factors (*r*) in ion mobility spectrometry, Anal. Chem. 72 (2000) 580–584.
[49] G.A. Eiceman, Z. Karpas, Ion Mobility Spectrometry, CRC press, Boca Raton, 2005.
[50] K.B. Shelimov, D.E. Clemmer, R.R. Hudgins, M.F. Jarrold, Protein structure in vacuo: gas-phase confirmations of BPTI and cytochrome *c*, J. Am. Chem. Soc. 119 (1997) 2240–2248.
[51] S.J. Valentine, J.G. Anderson, A.D. Ellington, D.E. Clemmer, Disulfide-intact and -reduced lysozyme in the gas phase: conformations and pathways of folding and unfolding, J. Phys. Chem. B 101 (1997) 3891–3900.
[52] S.L. Koeniger, D.E. Clemmer, Resolution and structural transitions of elongated states of ubiquitin, J. Am. Soc. Mass Spectrom. 18 (2007) 322–331.
[53] E.R. Badman, C.S. Hoaglund-Hyzer, D.E. Clemmer, Dissociation of different conformations of ubiquitin ions, J. Am. Soc. Mass Spectrom. 13 (2002) 719–723.
[54] C.F. Brandenburg, D.R. Latham, Spectroscopic identification of basic nitrogen compounds in Wilmington petroleum, J. Chem. Eng. Data 13 (1968) 391–394.
[55] A.M. Palumbo, G.E. Reid, Evaluation of gas-phase rearrangement and competing fragmentation reactions on protein phosphorylation site assignment using collision induced dissociation-MS/MS and MS^3, Anal. Chem. 80 (2008) 9735–9747.
[56] A. Devakumar, Y. Mechref, P. Kang, M.V. Novotny, J.P. Reilly, Identification of isomeric n-glycan structures by mass spectrometry with 157 nm laser-induced photofragmentation, J. Am. Soc. Mass Spectrom. 19 (2008) 1027–1040.